



Performance study of a rotary vane pressure exchanger for SWRO

Fanghua Ye, Jianqiang Deng*, Kai Liu, Zheng Cao

*School of Chemical Engineering and Technology, Xi'an Jiaotong University, Xi'an 710049, China,
Tel./Fax: +86 29 82663413; emails: dengjq@mail.xjtu.edu.cn (J. Deng), jkzx4416176@stu.xjtu.edu.cn (F. Ye),
liukaibk@stu.xjtu.edu.cn (K. Liu), czczkok@stu.xjtu.edu.cn (Z. Cao)*

Received 10 March 2017; Accepted 18 August 2017

ABSTRACT

In this study, models of a rotary vane pressure exchanger (RVPE) which is expected to be used as an energy recovery device in seawater reverse osmosis system were newly developed to study the performance of the proposed structure. The suitable design of the cylinder profile in RVPE was conducted. The leakage between brine stream and seawater stream, and the flow rate considering the leakage were studied. The contact performance between the cylinder and vane was discussed. Energy performance analysis was conducted to illustrate the energy saving potential of RVPE. The results show that the matching design of the cylinder profile and vane number can eliminate the short-circuit leakage and reversed flow, and reduce the energy loss in the energy recovery process. The interior leakage was controllable, and the flow rate presented periodic flow fluctuations. A careful selection of the device parameters, such as rotor speed, vane material density, vane thickness and vane radial length, is critical in order to ensure the contact performance between the cylinder and vane. According to the results, the RVPE is of reasonable structure, reliable performance and high energy saving potential to be a new type of energy recovery device.

Keywords: Pressure exchanger; Desalination; SWRO system; Energy recovery; Contact performance

1. Introduction

The demand of water resource is more and more serious due to the population growth and expanding industrial production scale. The seawater reverse osmosis (SWRO) technology has been proved as an effective method in seawater desalination to deal with the shortage of freshwater resources. In the SWRO technology, the application of energy recovery devices (ERDs) can obviously reduce the energy consumption and make the production of freshwater with low carbon emission [1]. The SWRO system coupled with ERDs includes a seawater supply pump, a high pressure pump, a booster pump, membrane modules and ERDs, as shown in Fig. 1.

Several kinds of ERDs have been developed for energy recovery [2]. They can be classified as the centrifugal ERDs [3,4] and positive displacement (PD) ERDs [5,6].

The centrifugal ERDs include the split ERDs and integrated ERDs. The split centrifugal ERDs mainly include the Francis turbine and Pelton impulse turbine (PIT). The Francis turbine is required to run nearly at the rated flow rate and suitable temperature. By contrast, the PIT is of higher energy recovery efficiency, and its efficiency varies slightly with the flow rate and operation pressure. But in the meantime, it is of complicated impeller structure and manufacture technique. An example of the integrated centrifugal ERDs is the hydraulic turbocharger. The energy recycle unit and pump body are located within the same shell, which reduces the mechanical transmission energy loss to some extent. In the centrifugal ERDs, the energy transfer process is completed by "hydraulic power to mechanical power to hydraulic power." In contrast, for the PD ERDs, the hydraulic power is transferred directly from brine stream to seawater stream. Hence, the PD ERDs is of higher work transfer efficiency than the centrifugal ERDs [7]. The common devices of the PD ERDs include

* Corresponding author.

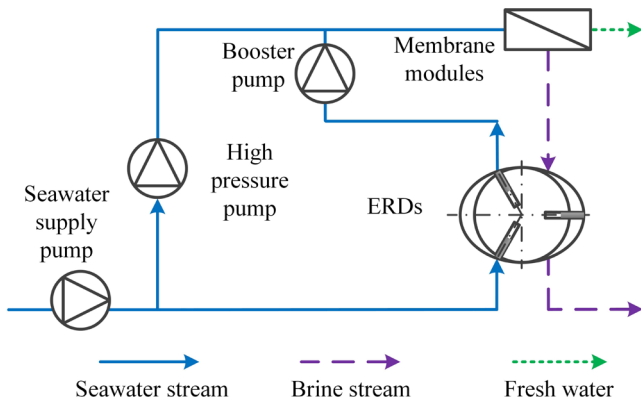


Fig. 1. SWRO system coupled with ERDs.

the piston-type work exchanger (PWE) and rotary pressure exchanger (RPE). The PWE is of high energy recovery efficiency and low fluid mixing rate. But its initial investment cost and maintenance cost are relatively high. Meanwhile, globe valves and servo valves are needed to precisely control the flow directions of fluid streams [8,9]. The RPE is of high efficiency, strong stability and low maintenance cost, which has been a critical component to decrease the energy cost in SWRO system [10,11]. Meanwhile, it is of difficult manufacture and serious fluid mixing [2,12]. In recent years, Al-Hawaj [13] has proposed a rotary vane pressure exchanger (RVPE) which was similar to a double-action sliding vane pump. Models for flow rate, friction and leakage loss, and efficiency of the device were presented based on the elliptic cylinder profile and under the assumption that each vane always contacted with the cylinder. It was found that the feasibility for the RVPE as an ERD highly depended on the friction loss and the leakage in the vane tip.

RVPE is a kind of rotary vane machines which mainly include rotary vane compressors, expanders and pumps. Rotary vane machines have been widely used because of their simple structure, easy manufacture, low cost and convenient operation. Much work has been conducted on the cylinder profiles, interior leakage, flow rate analysis, contact performance in the vane tip and device efficiency of rotary vane machines. Regarding cylinder profiles of rotary vane machines, Li et al. [14] compared the characteristics of a rotary vane compressor with different kinds of curves (elliptic curve, simple harmonic curve, cubic curve, etc.) as cylinder profiles. The shape of cylinder profile had great impact on the contact force, the seal performance between vanes and cylinder, the suction volume of compressor, and the pressure angles between vanes and cylinder. Song et al. [15] proposed the combined cylinder profile for a rotary vane compressor. The compressor with the combined cylinder profile had better vane motion characteristics, larger working volume and lower friction power than the compressor with harmonic cylinder profile theoretically. Experiments indicated that the test refrigeration cycle with the newly designed compressor had higher cooling capacity and coefficient of performance, and the newly designed compressor was of better performance in volumetric and isentropic efficiency. Jia et al. [16] showed that the larger eccentricity and vane incline angle of the cylinder profile in the rotary vane expander resulted in higher expander efficiency.

As to the interior leakage and flow rate within the device, Al-Hawaj [13] developed the mathematical model to study the leakage within RVPE. It is found that the leakage in the vane tip had a significant effect of the energy recovery performance of RVPE. Jia et al. [16] indicated that leakage through both the sealing arc and end clearances had a vital effect on the expander efficiency. Al-Hawaj [17] also investigated the interior leakage within the compressor by the proposed thermodynamic and dynamical mathematical models. The study illustrated the significant effect of leakage on power input requirement, discharge pressure and mass delivery, and less significant effect on mechanical efficiency and specific mass delivery. Lu et al. [18] developed the mathematics model to study the leakage flow of a rotary vane pump and compared with experimental results. Giuffrida and Lanzafame [19] proposed a mathematical model to determine the flow rate of a double-acting rotary vane pump. Lu et al. [20] experimentally tested the flow rate of the water vane pump and hydraulic vane motor.

With regard to the contact performance between the cylinder and vane, Lu et al. [18] studied the friction pair material, the structure and the vane tip contact force of a rotary vane pump by experimental test and mathematical model. The soft–hard material combinations presented superior friction characteristics. Yang et al. [21] showed that the tight contact between the cylinder and vane owing the springs arranged in the vane slots improved volumetric efficiency and isentropic efficiency of the rotary vane expander, and resulted in higher coefficient of performance in the transcritical CO₂ refrigeration cycle. Yang et al. [22] also established the mathematical model of vane dynamic of a CO₂ rotary vane expander to study the vane movement, especially the contact status between cylinder and vane, and validated the results with the pressure measurement experiment. The two adjacent vanes presented different movement behaviors, and adding springs in the vane bottom contributed to the tight contact between the cylinder and vane.

Towards the energy performance, especially for device efficiency, Bianchi and Cipollone [23] studied the friction power loss of a rotary vane compressor by experimental and modeling approaches. The improved configurations in vane mass, rotational speed and compressor aspect ratio can increase the compressor efficiency. Bianchi and Cipollone [24] also optimized geometrical and operation parameters of the rotary vane compressor to improve its mechanical efficiency. Inaguma and Hibi [25] theoretically and experimentally investigated the friction torque characteristics of the rotary vane pump, especially the friction torque characteristic between the vane tip and the cylinder wall and its influences on the mechanical efficiency. Lu et al. [20] introduced an integration of water vane pump and hydraulic vane motor in small reverse osmosis system, and the hydraulic vane motor was used as an ERD. The device efficiency and energy consumption have been experimentally investigated, and the results showed that the type of integration pump can decrease the system energy cost.

Much thorough research has been done on rotary vane compressors, expanders and pumps; but the study on RVPE is inadequate. As to RVPE, the problem of short-circuit leakage and reversed flow still occurs when the vane sweeps through outlet ports [13]. An accurate flow rate prediction with an appropriate model is still necessary to provide detailed flow

information in RVPE. The assumption that the vane always contacts with the cylinder has not been validated. Actually, the contact status between the cylinder and vane varies with the structural parameters and operation conditions. The prediction of the contact performance between the cylinder and vane is highly needed to guide the structural design of the device. Hence, in this paper, the suitable cylinder profile, which matched the number of vanes, was proposed. Then, a model focus on the leakage between brine stream and seawater stream was presented to study the leakage characteristics. The research on flow rate considering the leakage was conducted to investigate the flow rate characteristics. In addition, a vane dynamic model was developed to study the contact performance between the cylinder and vane. Finally, the energy performance analysis was conducted to illustrate the energy saving potential of RVPE.

2. Structural model

2.1. Cylinder profile

Fig. 2 shows the two-dimensional structure of the RVPE device. It consists of a circular rotor, a cylinder and several sliding vanes. The vane slots are evenly arranged in the cylinder, and the vane moves in respective vane slot. The rotor is inside the cylinder, which defines two crescent-shaped volumes. The volume at the brine side connects to high pressure (HP) brine inlet and low pressure (LP) brine outlet. The volume at the seawater side connects to LP seawater inlet and HP seawater outlet. The working theory of RVPE is simple: The HP brine stream pushes the vane to drive the rotor to rotate at brine side and entrains the LP seawater to HP pipe network at seawater side. The energy is transferred mechanically by the rotor and vane from brine stream to seawater stream.

The work transfer efficiency considering the flow rate difference between at the brine inlet, seawater inlet, brine outlet and seawater outlet can be described as:

$$\eta = \frac{P_{so}Q_{so} - P_{si}Q_{si}}{P_{bi}Q_{bi} - P_{bo}Q_{bo}} \quad (1)$$

where Q_{bi} , Q_{bo} , Q_{si} and Q_{so} are flow rates at the brine inlet, brine outlet, seawater inlet and seawater outlet, respectively, and other related parameters are shown in Table 1.

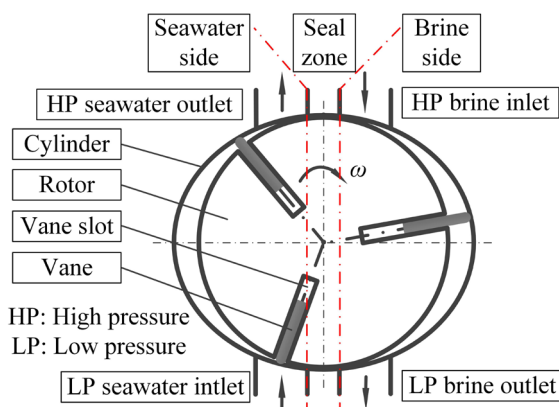


Fig. 2. Two-dimensional structure of RVPE.

Based on the device structure and working theory of RVPE, the design principle of the cylinder profile can be obtained as follows: (1) The seal performance between brine stream and seawater stream should be ensured to reduce the fluid mixing between brine stream and seawater stream. (2) The impact, vibration and operation noise of the vane is supposed to be controlled to a small value. It means that smooth and continuous cylinder profile must be adopted. (3) The tight contact between the cylinder and vane ought to be ensured. (4) The friction loss should be controlled to a small value, since the excessive friction loss would reduce the life and efficiency of the device.

In the RVPE device, the cylinder profile determines the characteristic of the cylinder inner contour, which is designed for the desired displacement of the vane. Fig. 3 presents the cylinder profile of RVPE at the seawater side. The cylinder profile at the brine side is symmetrical with that at the seawater side. As shown in Fig. 3, the cylinder profile consists of the seal section 1, inlet section, middle section, outlet section and seal section 2.

In the seal section 1 and seal section 2, each segment of cylinder profile is a circular arc whose radius is slightly larger than the radius of the rotor. The clearance fit between the rotor and the cylinder is adopted to reduce the leakage between brine stream and seawater stream. In the inlet section and outlet section, the cylinder profile characterized by high order polynomial is connected to the inlet port and outlet port, respectively. High order polynomial curves are conducive to the smooth mathematic continuity of cylinder profile to prevent unusual vibrational motions of the vane [19]. The middle section is the major part of the cylinder profile, which directly determines the fluid flow and the volume of the working chambers. The working chamber volume

Table 1
Default calculating parameter settings

Physical quantities	Parameters	Values
Short radius of cylinder profile, mm	R_1	70
Long radius of cylinder profile, mm	R_2	85
Rotor radius, mm	r	69.98
Clearance between rotor and cylinder in seal sections, mm	c	0.02
Angle, °	$\theta_0/\theta_1/\theta_2/\theta_3$	5/30/150/175
Vane density, $\text{kg}\cdot\text{m}^{-3}$	ρ	3,120
Vane thickness, mm	t	15
Vane radial length, mm	h	40
Vann tip friction coefficient	μ_1	0.05
Vane side friction coefficient	μ_2	0.05
Rotor speed, rpm	n	2,000
Number of vanes	N	3
Cylinder axial length, mm	b	30
Brine inlet pressure, MPa	P_{bi}	6.000
Brine outlet pressure, MPa	P_{bo}	0.300
Seawater inlet pressure, MPa	P_{si}	0.300
Seawater outlet pressure, MPa	P_{so}	5.715
Work transfer efficiency	η	0.95

should be relatively large, and the forces acting on the vane ought to be in good condition. Comparing several common profiles, such as elliptic profile, simple harmonic profile, double harmonic profile and parabolic profile, the characteristic of the simple harmonic profile is better than that of other profiles. So the simple harmonic profile is adopted in the middle section.

In this paper, seventh order polynomial curves are adopted in the inlet section and outlet section, which allows the continuity of the cylinder profile up to the third derivatives. According to the above description, the cylinder profile function can be written as:

$$\rho(\theta) = \begin{cases} R_1, (0 \leq \theta < \theta_0) \\ a_0 + a_1\theta + a_2\theta^2 + a_3\theta^3 + a_4\theta^4 + a_5\theta^5 + a_6\theta^6 + a_7\theta^7, (\theta_0 \leq \theta < \theta_1) \\ R_1 + (R_2 - R_1)\sin^2\theta, (\theta_1 \leq \theta < \theta_2) \\ a_8 + a_9\theta + a_{10}\theta^2 + a_{11}\theta^3 + a_{12}\theta^4 + a_{13}\theta^5 + a_{14}\theta^6 + a_{15}\theta^7, (\theta_2 \leq \theta < \theta_3) \\ R_1, (\theta_3 \leq \theta < \pi) \end{cases} \quad (2)$$

where the related parameters are shown in Table 1, and θ is angular position, $\rho(\theta)$ is radial coordinate of cylinder profile, the polynomial coefficients ($a_0 \sim a_{15}$) can be solved uniquely.

2.2. Number of vanes

The short circuit flow occurs if there are no vanes located in the middle section at brine side. Similarly, at seawater side, the LP seawater inlet is exposed to the HP seawater outlet if there are no vanes located in the middle section, leading to the reversed flow due to the HP differential. Although the check valve can be arranged downstream of the seawater inlet to prevent the reversed flow, it will add the complexity of the device and the flow resistance loss of the fluid. In addition, if there are more than one vane located in the middle section, the volume between the two adjacent vanes increases and then decreases when the vane sweeps through the middle section, which results in the energy loss in the decompression process of the liquid and possible damage of the device in the compression process of the liquid. So, only one vane should be always located in the middle section.

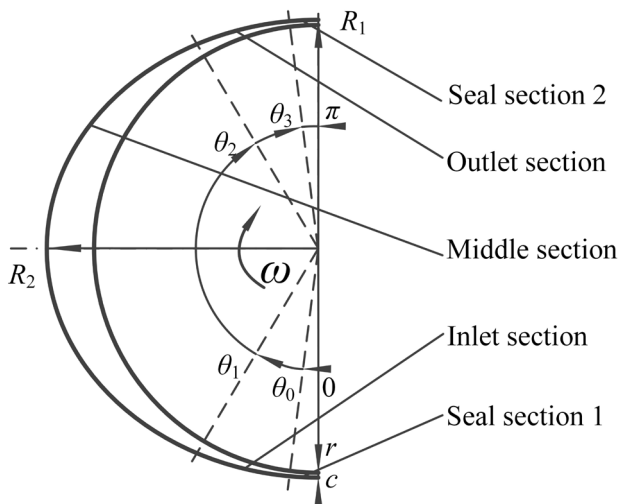


Fig. 3. Five-part form cylinder profile at the seawater side.

For double-vanes RVPE, the status that no vanes are located in the middle section will occur during the operation of the device. For three-vanes RVPE, the angle between the adjacent two vanes equals $2\pi/3$, and the cross angle of the middle section can be also designed to $2\pi/3$. In this case, there always exists only one vane located in the middle section at the brine side and the seawater side, respectively. Similarly, for four-vanes RVPE, the cross angle of the middle section should be designed to $\pi/2$. By that analogy, the reasonable vane number shall meet the conditions that the product of the number of the vane and the cross angle of the middle section is 2π . This matching design of the cylinder profile and vane number can eliminate the short-circuit leakage and reversed flow, and reduce the energy loss in the energy recovery process.

3. Interior leakage

Leakage within RVPE adds the fluid mixing between brine stream and seawater stream, and also leads to pressure loss in the energy recovery process. Fig. 4 displays the interior leakage paths in RVPE. Path 1 is the clearance between the cylinder inner wall and rotor outer wall in the seal sections, which can be divided into HP side seal section and LP side seal section, as shown in Fig. 4. Path 2 is the axial clearance between the end cover and rotor. The leakage occurs through path 3 between the cylinder wall and vane tip if the vane does not contact with the cylinder inner wall tightly. Path 4 is the axial clearance between the end cover and vane. The leakage occurs between two adjacent chambers through path 5 between the vane and vane slot.

Leakages in path 2, 4 and 5 can be controlled to be practically small by appropriate structural design of the device. The leakage in path 3 can be eliminated by ensuring the tight contact between the cylinder and vane in middle section, which will be discussed below in this paper. With regard to the leakage in path 1, a length of sealing circular arc whose radius is slightly larger than the rotor radius is arranged in the cylinder inner wall to control the leakage clearance and leakage length. The leakage rate can be obtained by simplifying the leakage passage into the clearance between two parallel plates of relative motion. Fig. 5 shows the simplified leakage flow model in seal sections. The cylinder inner wall is regarded as the stationary nether flat, and the rotor outer wall is regarded as the moving upper flat with a speed of U in the x direction. The movement of the upper flat is referred as

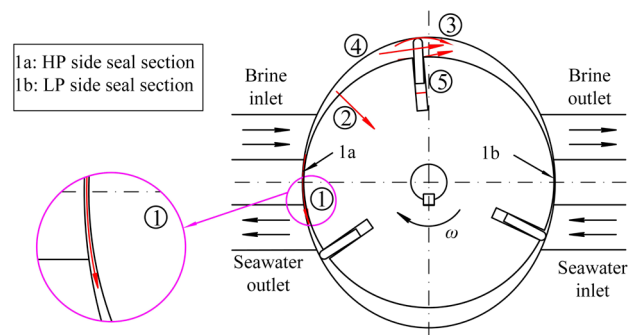


Fig. 4. Interior leakage paths within RVPE.

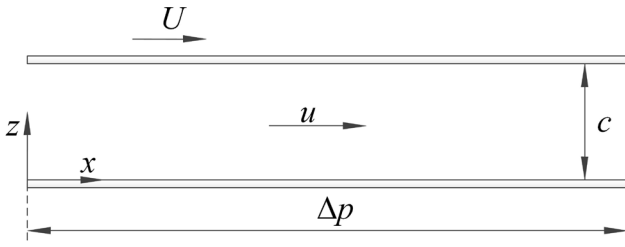


Fig. 5. The simplified leakage flow model in seal sections.

the rotation of the rotor relative to the cylinder. The clearance between nether plate and upper plate equals c , and the pressure difference between the two ends of the leakage channel equals Δp . The boundary conditions are: $z = 0, u = 0$; $z = c, u = U$.

Reynolds equation can be written as:

$$\frac{\partial}{\partial x} \left(\frac{\rho c^3}{12\mu} \frac{\partial p}{\partial x} \right) + \frac{\partial}{\partial y} \left(\frac{\rho c^3}{12\mu} \frac{\partial p}{\partial y} \right) = \frac{\partial}{\partial x} \left(\frac{\rho c u}{2} \right) + \frac{\partial(\rho c)}{\partial t} + \frac{\partial p}{\partial t} \quad (3)$$

Taking the assumption that liquid is incompressible and the liquid flows only in the x direction, the above equation can be simplified as one-dimensional Reynolds equation:

$$\frac{\partial}{\partial x} \left(c^3 \frac{\partial p}{\partial x} \right) = 6\mu u \frac{\partial c}{\partial x} \quad (4)$$

Substituting the boundary conditions, the flow velocity of the fluid can be obtained:

$$u = -\frac{c^2}{2\mu} \frac{\partial p}{\partial x} \left[\frac{z}{c} - \left(\frac{z}{c} \right)^2 \right] + U \frac{z}{c} \quad (5)$$

where the velocity is made up of two items. The former is the flow velocity caused by the pressure difference, and the latter is the flow velocity caused by the shear action of the rotor outer wall.

Assuming that the pressure drop is evenly distributed in the x direction, the average flow velocity and the volumetric flow rate can be acquired, respectively:

$$u_m = -\frac{1}{c} \int_0^c u dz = -\frac{c^2}{12\mu} \frac{\partial p}{\partial x} + \frac{U}{2} \quad (6)$$

$$Q_l = b \int_0^c u dz = \frac{bc^3}{12\mu} \frac{\partial p}{\partial x} + \frac{Uhb}{2} \quad (7)$$

Fig. 6 shows the effect of clearance on the leakage flow rate with a constant rotor speed of 2,000 rpm. As Fig. 6 shows, at the LP side seal section, brine leaks into seawater, and the leakage flow rate increases linearly when the clearance is 0–0.05 mm. While at the HP side seal section, seawater leaks into brine and then brine leaks into seawater when the clearance is 0–0.05 mm. With an increasing clearance, the leakage flow rate increases and reaches a maximum, and then reduces to a negative value. Fig. 7 presents the effect of the

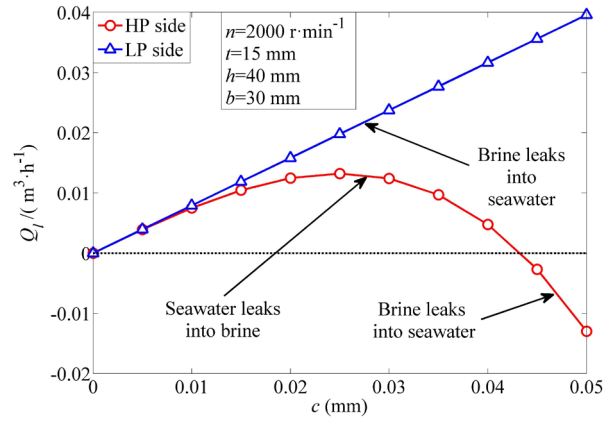


Fig. 6. Effect of clearance on leakage flow rate.

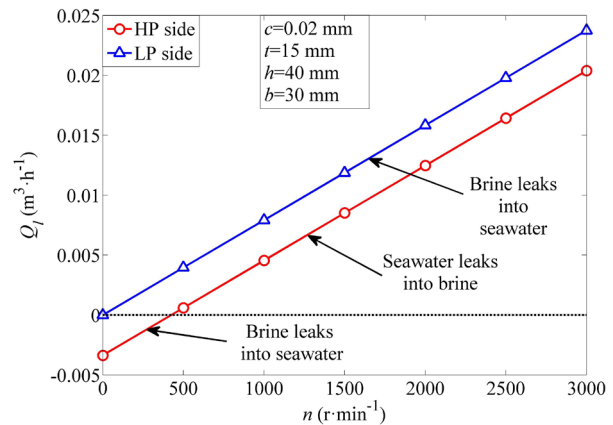


Fig. 7. Effect of rotor speed on leakage flow rate.

rotor speed on the leakage flow rate with a constant clearance of 0.02 mm. As shown in Fig. 7, at the LP side seal section, brine leaks into seawater, and the leakage flow rate increases with the rotor speed linearly. While at the HP side seal section, brine leaks into seawater and then seawater leaks into brine when the rotor speed is from 0 to 3,000 rpm. The leakage flow rate increases with the rotor speed linearly from a negative value to a positive value.

Theoretically, the leakage characteristic can be improved by the adjustment of the clearance and the rotor speed. Actually, with a rotor speed of 2,000 rpm and a clearance of 0.02 mm, the leakage flow rate that seawater leaks into brine accounts for the brine inlet flow rate 0.069% at the HP side seal section. While at the LP side seal section, the leakage flow rate that brine leaks into seawater accounts for the seawater inlet flow rate 0.088%. The flow rate of the leakage is rather small when compared with the flow rate of the device, indicating that the leakage flow rate in the device is controllable.

4. Flow rate prediction

The flow rate characteristic is closely related to the work transfer between brine stream and seawater stream. Regardless of the leakage between brine stream and seawater

stream, the flow rate in RVPE only relates to the cylinder profile and rotor speed. It is assumed that the vane contacts with the cylinder in the middle of the semicircular vane tip, and the rotor rotates in the clockwise direction with a constant speed. The clearance between the vane side and the vane slot is neglected, since it is too small when compared with the vane thickness.

Fig. 8 displays the initial position of a vane and its position after $d\theta$ angular rotation. And Fig. 9 presents the partial enlarged view close to the rotor center. As presented in Figs. 8 and 9, if θ locates the vane axis in the initial position, then the vane axis in the new position is located by the angle $\theta + d\theta$. The vane contacts with the cylinder at the point T . The point E is the intersection point of the vane left side and rotor outer contour. The point M is the intersection point of the vane left side and vane tip contour. The point N is the intersection point of the prolongation of the vane left side and cylinder inner contour. It is found that the prolongation of the segment NE is tangent to a circle whose radius equals half of vane thickness and circle center lies in the rotor center. The tangent point lies in the point P . The curve TME and the vane axis OT have moved to $T_iM_iE_i$ and OT_i , respectively, during the $d\theta$ angular rotation. The point J is the intersection point of the prolongation of the segment NP and the prolongation of the segment N_iP_i . The subscript i stands for the new position.

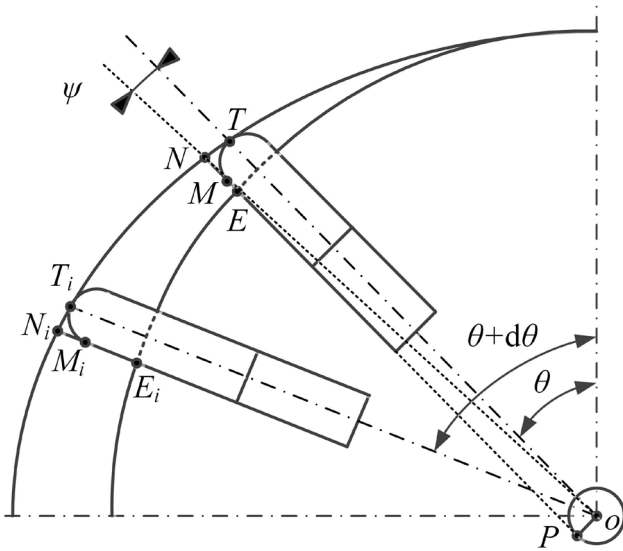


Fig. 8. The initial position of a vane and its position after $d\theta$ angular rotation.

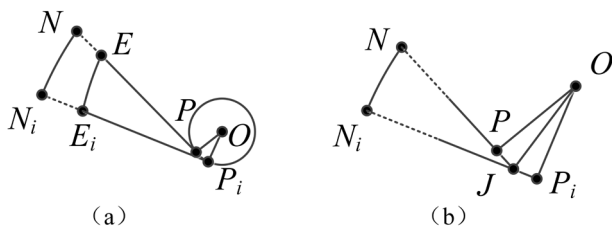


Fig. 9. Partial enlarged view close to the rotor center.

The angle ψ is the angle between the straight line ON and the axis of the vane, which is determined by solving an implicit function:

$$\rho(\theta + \psi) \sin \psi = t / 2 \tag{8}$$

The volume of the discharged fluid during the $d\theta$ angular rotation can be evaluated as:

$$dA(\theta) = A_{NEE_iN_iN} + A_{NETN} - A_{N_iE_iT_iN_i} \tag{9}$$

where the subscripts stand for the closed zone, and A is the area of the closed zone. The representations method is also applied in the flowing equations.

The first item on the right in Eq. (9) can be calculated as:

$$A_{NEE_iN_iN} = A_{N_iN_iN} - A_{E_iE_iE} \tag{10}$$

where

$$A_{N_iN_iN} = \frac{1}{2} \overline{NJ}^2 d\theta = \frac{1}{2} \left[\overline{NP} + \left(\frac{t}{2} \frac{d\theta}{2} \right) \right]^2 d\theta \tag{11}$$

$$A_{E_iE_iE} = \frac{1}{2} \overline{EJ}^2 d\theta = \frac{1}{2} \left[\overline{EP} + \left(\frac{t}{2} \frac{d\theta}{2} \right) \right]^2 d\theta \tag{12}$$

Neglecting the infinitesimal of the order greater than the first, it is possible from Eqs. (10)–(12) to come to Eq. (13):

$$A_{NEE_iN_iN} = \frac{1}{2} (\overline{NP}(\theta)^2 - \overline{EP}(\theta)^2) d\theta \tag{13}$$

where

$$\overline{NP}(\theta) = \left[\rho(\theta + \psi)^2 - (t/2)^2 \right]^{1/2} \tag{14}$$

$$\overline{EP}(\theta) = \left[r^2 - (t/2)^2 \right]^{1/2} \tag{15}$$

The latter two items on the right in Eq. (9) can be expressed as:

$$A_{NETN} - A_{N_iE_iT_iN_i} = -dA_{NETN} \tag{16}$$

The closed region A_{NETN} can be divided into four parts:

$$A_{NETN}(\theta) = A_{OTNO}(\theta) + A_{ONPO}(\theta) - A_{OGMPO}(\theta) - A_{GRMG}(\theta) \tag{17}$$

then

$$A_{NETN}(\theta) = \int_0^{\theta+\psi} \frac{1}{2} (\rho(\theta))^2 d\theta + \frac{1}{2} \rho(\theta + \psi) \cos \psi \frac{t}{2} - \left(\rho(\theta) - \frac{t}{2} \right) \frac{t}{2} - \frac{1}{4} \pi \left(\frac{t}{2} \right)^2 \tag{18}$$

Taking the vane axial length into account, the ideal flow rate Q_{id} can be written:

$$Q_{id}(\theta) = \omega b \cdot \frac{dA(\theta)}{d\theta} \quad (19)$$

Considering the leakage between the two fluid streams, the flow rates at brine inlet, brine outlet, seawater inlet and seawater outlet can be expressed as follows:

$$Q_{bi} = Q_{so} = Q_{id} - Q_{hl} \quad (20)$$

$$Q_{bo} = Q_{si} = Q_{id} - Q_{ll} \quad (21)$$

where Q_{hl} is the leakage flow rate at the HP side and Q_{ll} is the leakage flow rate at the LP side.

The outlet flow rates, especially the seawater outlet flow rate is the primary concern variable. Fig. 10 shows the instantaneous flow rate at the brine outlet and the seawater outlet with a vane thickness of 15 mm and a rotor speed of 2,000 rpm. It can be observed from the figure that the seawater outlet flow rate Q_{so} and brine outlet flow rate Q_{bo} all present periodic flow fluctuations with a cycle of $2\pi/3$ which equals the cross angle of the middle section. The variation trends of the seawater outlet flow rate Q_{so} and the brine outlet flow rate Q_{bo} are similar. The mutation of the flow rate occurs at its minimum value. This is due to the mutation of the chamber volume between the two adjacent vanes when the leading vane leaves the middle section and the trailing vane enters the middle section. Efforts should be made to reduce the flow fluctuation, such as multi-rotor arrangement [13]. Multiple rotors operate in parallel and are synchronized to a same shaft with equally distributed vane angular shift. Fig. 11 presents the flow rate at seawater outlet for k -rotor arrangement RVPE. As shown in Fig. 11, the arrangement of multi-rotor can obviously decreases the flow fluctuation. Specifically, the four-rotor arrangement decreases flow fluctuation to lower than 8.4% of the main flow over the course of the rotor rotation. Meanwhile, the multi-rotor arrangement decreases the period of the flow fluctuation. It should be pointed out that the multi-rotor arrangement has a similar effect on the flow fluctuation at brine inlet, brine outlet and seawater inlet.

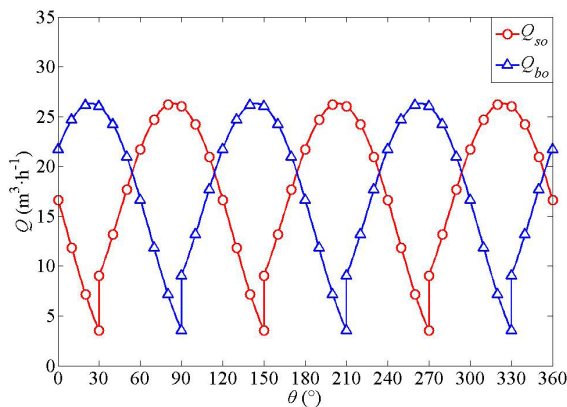


Fig. 10. The flow rate at brine outlet and seawater outlet.

5. Contact performance

The contact performance between the cylinder and vane has a vital impact on the work transfer process between brine stream and seawater stream, and can eliminate the leakage in the vane tip. Fig. 12 presents the forces acting on the vane. The vane bears the gravitational force F_g , the coriolis inertial force $F_{k'}$, the centrifugal inertial force F_r , the convected inertial force $F_{e'}$, the force F_b acting on the vane bottom caused by the liquid in the vane slot, the force F_p acting on the vane side caused by the liquid pressure difference between the two sides of the vane, the forces F_{pt1} and F_{pt2} acting on the vane tip caused by the liquid in the vane tip, the contact force F_{nt} in the vane tip, the contact forces F_{n1} and F_{n2} at the two sides of the vane, the friction force F_{ft} in the vane tip, the friction force F_{f1} and F_{f2} at the two sides of the vane. The inertia forces, F_e , F_r and $F_{k'}$ are obtained according to vane kinematics. The forces, $F_{e'}$, $F_{b'}$, $F_{p1'}$, F_{p11} and $F_{p12'}$ are related to the pressure of the liquid at two sides of the vane and in the vane slot at the given angle. The forces, $F_{n1'}$, $F_{n2'}$, $F_{nt'}$, $F_{f1'}$, F_{f2} and $F_{ft'}$ are obtained by solving the force equilibrium equations. The contact status

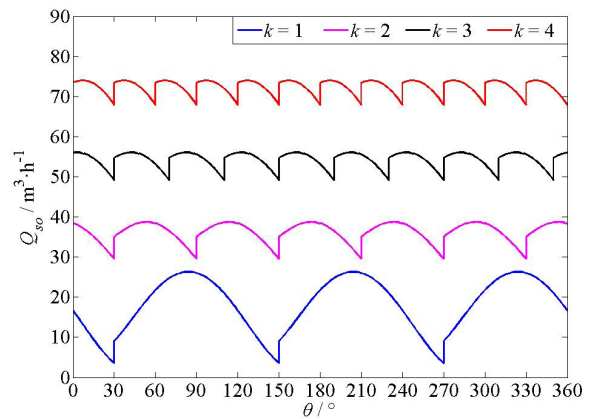


Fig. 11. Flow rate at seawater outlet for k -rotor arrangement RVPE.

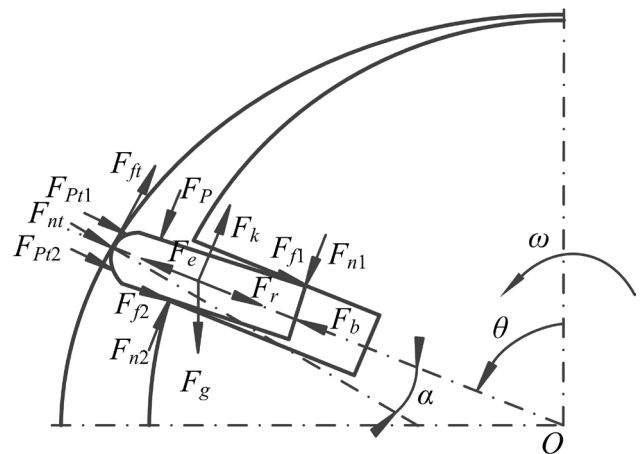


Fig. 12. Forces acting on the vane.

between the cylinder and the vane can be identified by the calculated results. It is concluded that the vane tightly contacts with the cylinder if the contact force F_{nt} is positive. But if the contact force F_{nt} is zero or negative, it is concluded that the vane does not contact with the cylinder. The following assumptions are under consideration: (1) The rotor, cylinder and vane are rigid without wear. (2) The contact forces act along the surface of the vane uniformly in the axial direction.

Since the direction of the centrifugal inertia force F_r , the coriolis inertia force F_k , the frictional forces F_{f1} and F_{f2} are associated with the direction of vane velocity relative to the rotor, the forces acting on the vane should be all separated into two cases, that is, the case that the rotation angle ranged from 0 to $\pi/2$ and the case that the rotation angle ranged from $\pi/2$ to π . But the two cases can be expressed as a uniform formula by introducing a sign function.

If the vane contacts with the cylinder, the force equilibrium equation can be written as:

$$\begin{pmatrix} -\cos\alpha - \mu_1 \sin\alpha & -\mu_2 \text{sign}(v_r) & -\mu_2 \text{sign}(v_r) \\ \sin\alpha - \mu_1 \cos\alpha & 1 & -1 \\ (\sin\alpha - \mu_1 \cos\alpha)h/2 & -h/2 - \mu_2 \text{sign}(v_r)t/2 & -(h/2 - l) + \mu_2 \text{sign}(v_r)t/2 \end{pmatrix} \begin{pmatrix} F_{nt} \\ F_{n1} \\ F_{n2} \end{pmatrix} \quad (22)$$

$$= \begin{pmatrix} -F_c + F_r + F_g \sin\theta - F_b + F_{pt1} + F_{pt2} \\ F_k + F_g \cos\theta - F_p \\ -F_p(h-l)/2 + F_{pt1}t/4 - F_{pt2}t/4 \end{pmatrix}$$

where l is the vane radius length out of the vane slot, α is the inclined angle between the vane axis and the normal line at the contact point between the cylinder and vane, v_r is the

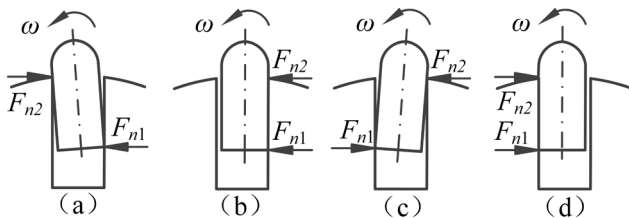


Fig. 13. The tilt state of the vane during the movement.

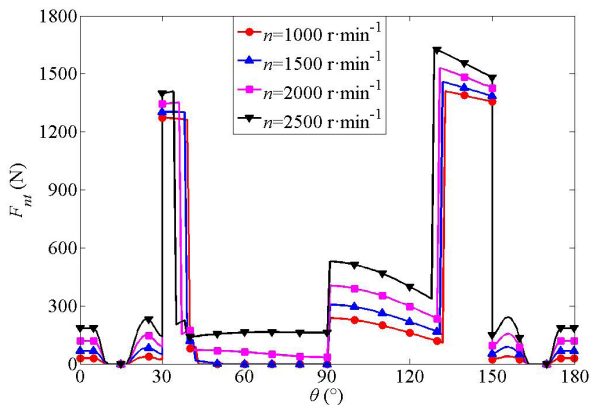


Fig. 14. Effect of rotor speed on vane tip contact force at the seawater side.

vane velocity relative to the rotor and other related parameters are shown in Table 1.

If the vane does not contact with the cylinder, the contact forces at the vane sides are obtained by:

$$F_{n1} = \frac{(-F_c + F_r + F_g \sin\theta - F_b + F_{pt})t/2 + (F_k + F_g \cos\theta)\left(-\frac{h}{2} + l\right) - F_p \frac{l}{2}}{-h + l - \mu_2 \text{sign}(v_r)t} \quad (23)$$

$$F_{n2} = F_{n1} - F_k - F_g \cos\theta + F_p \quad (24)$$

The size of F_{n1} and F_{n2} reflects the tilt status of the vane. If $F_{n1} > 0$ and $F_{n2} > 0$, the vane is in the forward-leaning state shown in Fig. 13(a). If $F_{n1} > 0$ and $F_{n2} \leq 0$, the vane contacts with the rear surface of the vane slot shown in Fig. 13(b). If $F_{n1} \leq 0$ and $F_{n2} \leq 0$, the vane is in the backward-leaning state shown in Fig. 13(c). If $F_{n1} \leq 0$ and $F_{n2} > 0$, the vane contacts with the front surface of the vane slot shown in Fig. 13(d). If the vane contacts with the rear surface of the vane slot, the vane slot bottom connects the front chamber, so the pressure of the fluid on the vane slot bottom equals that in the front chamber.

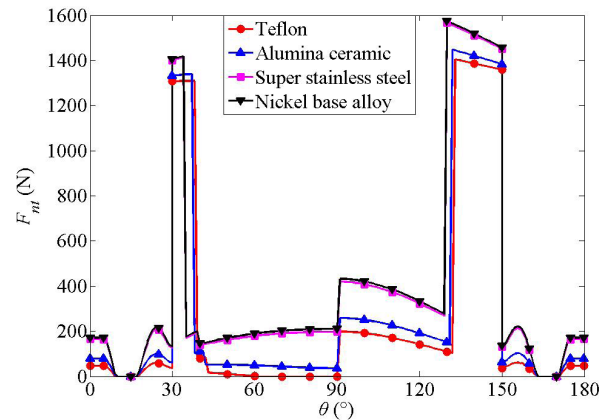


Fig. 15. Effect of vane material on vane tip contact force at the seawater side.

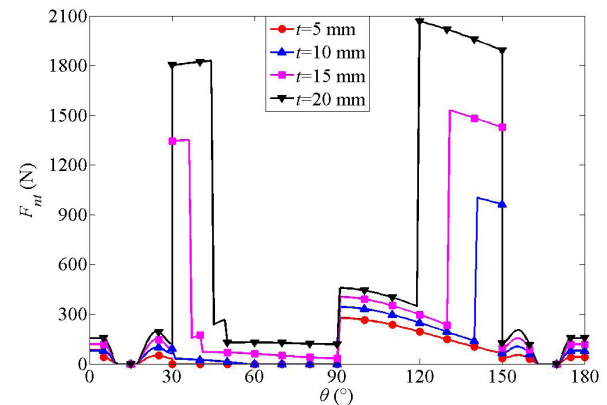


Fig. 16. Effect of vane thickness on vane tip contact force at the seawater side.

If the vane contacts with the front surface of the vane slot, the pressure of the fluid on the vane slot bottom equals that in the near chamber. If the vane is in the forward-leaning state or in the backward-leaning state, the pressure of the fluid on the vane slot bottom equals the average value of the liquid pressure between in the front chamber and near chamber.

The contact performance between the cylinder and vane is characterized by the value of the contact force F_{nt} in the vane tip. Figs. 14–17 display the influences of the rotor speed, vane material, vane thickness and vane radial length on the vane tip contact force F_{nt} between the cylinder and vane at the seawater side. From these figures, the trends that the contact force changing with the angle are almost the same. In the seal section 1 and the seal section 2, the contact force is positive and remains constant. The contact force fluctuation occurs in the inlet section and the outlet section, because the polynomial curve profile can only guarantee the finite order mathematical continuity of the profile. In the middle section, several mutations of the contact force occur due to the change in the direction of the frictional forces, F_{f1} and F_{f2} , and the transition of the vane tilt state. Calculation results of the contact force at the brine side are similar to that at the seawater side, so this paper only presents the specific results at the seawater side.

In Figs. 14–17, the status that the vane tip contact force F_{nt} equals to zero occurs in the middle section, the inlet section and the outlet section. It is not necessary to ensure that the vane contacts with the cylinder in the inlet and outlet sections, so zero value of the contact force in the vane tip are acceptable. But in the middle section, in order to ensure efficient work transfer process, the tight contact between the cylinder and vane should be ensured, thus the status of zero values of the contact force should be avoided.

The conditions that the vane cannot contact with the cylinder are prone to occur at the angle of 30° – 90° , especially close to 90° . This is because the small variation rate in the diameter of the cylinder profile leads to small values of the inertia force F_r , the inertia force F_v , the frictional forces F_{f1} and F_{f2} , which is not conducive to the tight contact between the cylinder and vane. As shown in Fig. 14, the vane tip contact force increases with the rotor speed as a whole, which is beneficial to the tight contact between the cylinder and vane in the middle section. As shown in Fig. 15, if the vane is made

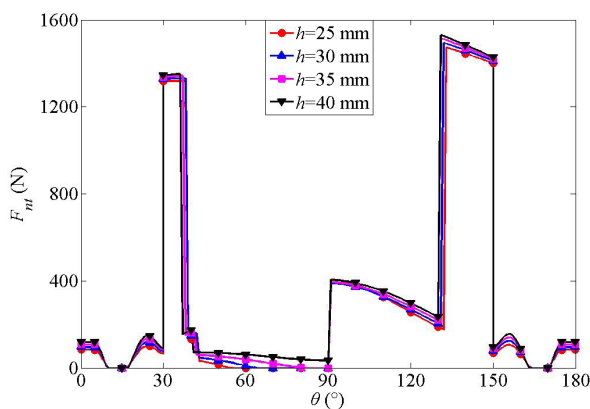


Fig. 17. Effect of vane radial length on vane tip contact force at the seawater side.

of light material such as Teflon, the vane cannot always contact with the cylinder when the vane goes through the middle section. On the contrary, if the vane is made of heavy material such as alumina ceramic, super stainless steel and nickel base alloy, the vane can always contact with cylinder in the middle section. Figs. 16 and 17 show that increasing the vane thickness and vane radial length are all beneficial to the tight contact between the cylinder and vane in the middle section. The study above mentioned shows that the specific vane structure and the rotor speed can be reasonably designed to improve the contact performance between the cylinder and vane in the middle section.

6. Energy performance analysis

Considering hydrodynamically lubricated conditions, the energy performance analysis is conducted to illustrate the energy saving potential of RVPE with parameters shown in Table 1. In this study, the work transfer efficiency is firstly assumed as a constant value of 95%. With the variation of the rotor speed, vane material density, vane thickness and vane radial length, the vane friction loss, which is the main energy loss in the energy recovery process, accounts for the output power in brine side of 1.88% to 3.65%. It indicates that the vane friction loss is within the range of the energy loss according to the designed work transfer efficiency. Hence, the designed value 95% of the work transfer efficiency of RVPE is reasonable.

Fig. 18 shows the SWRO system without ERDs. The seawater stream is pressurized from P_0 to P_s by a HP pump to overcome the transmembrane osmotic pressure. The work done by the HP pump is expressed as:

$$W_{hp} = \frac{Q_s(P_s - P_0)}{\eta_{hp}} \quad (25)$$

where W_{hp} is the work done by HP pump, P_0 is the pressure at the entrance of HP pump, P_s is the pressure at the exit of HP pump, η_{hp} is the HP pump efficiency.

The specific energy consumption is defined as the electrical energy request per unit of freshwater. Then, the specific energy consumption for the SWRO system without ERDs is evaluated by:

$$SEC_0 = \frac{W_{hp}}{Q_f} = \frac{Q_s(P_s - P_0)}{Q_f \eta_{hp}} \quad (26)$$

where SEC_0 is the specific energy consumption for the SWRO system without ERDs, Q_f is the flow rate of freshwater.

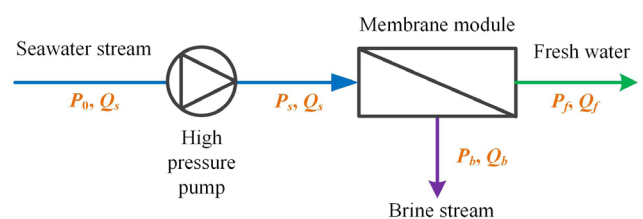


Fig. 18. Schematic of SWRO system without ERDs.

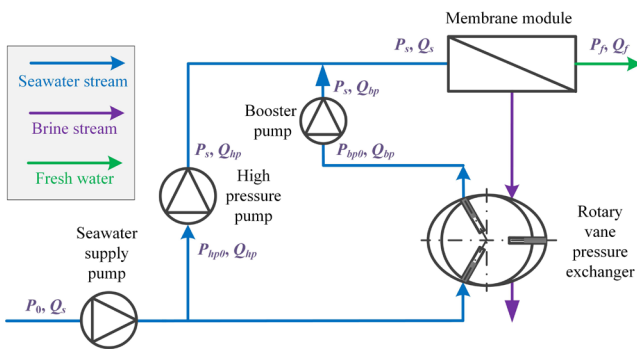


Fig. 19. Schematic of SWRO system with a RVPE device.

Fig. 19 shows the SWRO system with a single RVPE device. The brine stream discharged from the membrane module with HP is used to pressurize a part of seawater stream. Hence, the pressure energy in the brine stream is used in cycle, and the total energy consumption is reduced. The energy consumption in the SWRO system includes seawater supply pump work, HP pump work and booster pump work, which can be evaluated by:

$$W_{ss} = \frac{Q_{ss}(P_{hp0} - P_0)}{\eta_{ss}} \quad (27)$$

$$W_{hp} = \frac{Q_{hp}(P_s - P_{hp0})}{\eta_{hp}} \quad (28)$$

$$W_{bp} = \frac{Q_{bp}(P_s - P_{bp0})}{\eta_{bp}} \quad (29)$$

where W_{ss} , W_{hp} and W_{bp} are the work done by the seawater supply pump, HP pump and booster pump respectively; Q_{ss} , Q_{hp} and Q_{bp} are the volumetric flow rate of the seawater supply pump, HP pump and booster pump, respectively; η_{ss} , η_{hp} and η_{bp} are the efficiencies of the seawater supply pump, HP pump and booster pump, respectively; P_0 is the pressure at the entrance of the seawater supply pump; P_{hp0} is the pressure at the entrance of the HP pump (equals the pressure at the exit of the seawater supply pump); P_s is the pressure of seawater stream at the entrance of the membrane module.

The specific energy consumption for the SWRO system with a RVPE is defined as:

$$SEC_1 = \frac{W_{ss} + W_{hp} + W_{bp}}{Q_f} \quad (30)$$

$$= \frac{1}{Q_f} \left(\frac{Q_{ss}(P_{hp0} - P_0)}{\eta_{ss}} + \frac{Q_{hp}(P_s - P_{hp0})}{\eta_{hp}} + \frac{Q_{bp}(P_s - P_{bp0})}{\eta_{bp}} \right)$$

where SEC_1 is the specific energy consumption of the SWRO system with a RVPE device, Q_f is the flow rate of freshwater.

Consider a SWRO system in the presence of a single RVPE device with parameters in Table 1, then $Q_{bp} = 18.09 \text{ m}^3 \cdot \text{h}^{-1}$, $P_0 = 0.100 \text{ MPa}$, $P_{hp0} = 0.300 \text{ MPa}$, $P_{bp0} = 5.715 \text{ MPa}$, $P_s = 6.000 \text{ MPa}$. With the target recovery rate of 0.4, the flow rates of seawater

supply pump Q_{ss} , HP pump Q_{hp} and freshwater Q_f are 30.15, 12.06 and 12.06 $\text{m}^3 \cdot \text{h}^{-1}$, respectively. Assuming $\eta_{hp} = 0.80$, $\eta_{ss} = 0.85$, $\eta_{bp} = 0.85$, the specific energy consumption SEC_1 can be calculated by:

$$SEC_1 = \frac{1}{12.06} \left(\frac{30.15(0.3 - 0.1)}{0.85} + \frac{12.06(6 - 0.3)}{0.8} + \frac{18.09(6 - 5.715)}{0.85} \right) \quad (31)$$

$$\frac{1000}{3600} = 2.282 \text{ kWh} \cdot \text{m}^{-3}$$

While, regarding a SWRO system in the absence of ERDs shown in Fig. 18, the specific energy consumption SEC_0 is solved by:

$$SEC_0 = \frac{30.15(6 - 0.1)}{12.06 \times 0.8} \frac{1000}{3.6} = 5.122 \text{ kWh} \cdot \text{m}^{-3} \quad (32)$$

According to the calculation results, the specific energy consumption decreases from 5.122 to 2.282 $\text{kWh} \cdot \text{m}^{-3}$ by introducing the RVPE. Considering the current specific energy consumption in the SWRO system which is 2–3 $\text{kWh} \cdot \text{m}^{-3}$ [26–28], the calculation of the specific energy consumption in our results is reasonable. Moreover, with the multi-rotor RVPE devices used in the SWRO system, the reduction of the energy consumption will increase multiply.

7. Conclusions

In this study, a theoretical approach was applied to study the leakage, flow rate, contact performance and energy performance of RVPE based on the proposed structural model. The three-vane RVPE matched with the five-part cylinder profile is designed and used to carry out the following analysis. The leakage flow rates between the brine stream and the seawater stream is controllable and can be ignored when compared with the inlet flow rates. The instantaneous flow rate presents periodic flow fluctuations with a cycle which equals the cross angle of the middle section. The multi-rotor arrangement can significantly decrease the flow fluctuation which is of vital importance for the practical application of RVPE. Increasing rotor speed, vane material density, vane thickness and vane radial length are all beneficial for contact performance between the cylinder and vane. The application of RVPE in the SWRO system can obviously decrease the energy consumption theoretically. The results present considerable potential of the RVPE as an efficient ERD for the SWRO system.

Acknowledgment

This work was supported by the National Natural Science Foundation of China (Grant No. 21376187).

References

- [1] A.M. Farooque, A.T.M. Jamaluddin, A.R. Al-Reweli, P.A.M. Jalaluddin, S.M. Al-Marwani, A.A. Al-Mobayed, A.H. Qasim, Parametric analyses of energy consumption and losses in SWCC SWRO plants utilizing energy recovery devices, *Desalination*, 219 (2008) 137–159.
- [2] R.L. Stover, Development of a fourth generation energy recovery device. A "CTO's notebook," *Desalination*, 165 (2004) 313–321.

- [3] E. Oklejas, W.F. Pergande, Integration of advanced high-pressure pumps and energy recovery equipment yields reduced capital and operating costs of seawater RO systems, *Desalination*, 127 (2000) 181–188.
- [4] T. Manth, M. Gabor, E. Oklejas, Minimizing RO energy consumption under variable conditions of operation, *Desalination*, 157 (2003) 9–21.
- [5] E. Xu, Y. Wang, J. Wu, S. Xu, Y. Wang, S. Wang, Investigations on the applicability of hydrostatic bearing technology in a rotary energy recovery device through CFD simulation and validating experiment, *Desalination*, 383 (2016) 60–67.
- [6] R.L. Stover, J. Martin, Reverse osmosis and osmotic power generation with isobaric energy recovery, *Desal. Wat. Treat.*, 15 (2010) 267–270.
- [7] R.L. Stover, Retrofits to improve desalination plants, *Desal. Wat. Treat.*, 13 (2010) 33–41.
- [8] J. Sun, Y. Wang, S. Xu, S. Wang, Energy recovery device with a fluid switcher for seawater reverse osmosis system, *Chin. J. Chem. Eng.*, 16 (2008) 329–332.
- [9] X. Wang, Y. Wang, J. Wang, S. Xu, Y. Wang, S. Wang, Comparative study on stand-alone and parallel operating schemes of energy recovery device for SWRO system, *Desalination*, 254 (2010) 170–174.
- [10] A. Zhu, P.D. Christofides, Y. Cohen, Effect of thermodynamic restriction on energy cost optimization of RO membrane water desalination, *Ind. Eng. Chem. Res.*, 48 (2009) 6010–6021.
- [11] A. Zhu, P.D. Christofides, Y. Cohen, Minimization of energy consumption for a two-pass membrane desalination: effect of energy recovery, membrane rejection and retentate recycling, *J. Membr. Sci.*, 339 (2009) 126–137.
- [12] Z. Yihui, D. Xinwei, J. Maowei, C. Yuqing, Numerical simulation on a dynamic mixing process in ducts of a rotary pressure exchanger for SWRO, *Desal. Wat. Treat.*, 1 (2009) 107–113.
- [13] O.M. Al-Hawaj, Theoretical analysis of sliding vane energy recovery device, *Desal. Wat. Treat.*, 36 (2011) 354–362.
- [14] L. Li, Y. Zhao, B. Guo, P. Shu, J. Shen, S. He, Wrap of cylinder and its effect on main features of rotary vane compressor for automobile air conditioning system, *Int. J. Refrig.*, 26 (2003) 566–574.
- [15] L. Song, L. Zeng, J. Zhou, X. Luo, Profile design for the cylinder of a double-acting rotary vane compressor, *Proc. Inst. Mech. Eng., Part C: J. Mech. Eng. Sci.*, 230 (2016) 2300–2313.
- [16] X. Jia, B. Zhang, B. Yang, X. Peng, Study of a rotary vane expander for the transcritical CO₂ Cycle—Part II: theoretical modeling, *HVAC&R Res.*, 15 (2009) 689–709.
- [17] O. Al-Hawaj, Theoretical modeling of sliding vane compressor with leakage, *Int. J. Refrig.*, 32 (2009) 1555–1562.
- [18] Y. Lu, W. Zhang, Y. Zhao, Z. Wang, P. Shu, Studies on several key problems of water hydraulic vane pump, *Ind. Lubr. Tribol.*, 63 (2011) 134–141.
- [19] A. Giuffrida, R. Lanzafame, Cam shape and theoretical flow rate in balanced vane pumps, *Mech. Mach. Theory*, 40 (2005) 353–369.
- [20] Y. Lu, Y. Zhao, G. Bu, P. Shu, The integration of water vane pump and hydraulic vane motor for a small desalination system, *Desalination*, 276 (2011) 60–65.
- [21] B. Yang, X. Peng, S. Sun, B. Guo, Z. Xing, Study of a rotary vane expander for the transcritical CO₂ cycle—Part I: experimental investigation, *HVAC&R Res.*, 15 (2009) 673–688.
- [22] B. Yang, X. Peng, S. Sun, B. Guo, Z. Xing, A study of the vane dynamics in a rotary vane expander for the transcritical CO₂ refrigeration cycle, *Proc. Inst. Mech. Eng., Part A: J. Power Energy*, 223 (2009) 429–440.
- [23] G. Bianchi, R. Cipollone, Friction power modeling and measurements in sliding vane rotary compressors, *Appl. Therm. Eng.*, 84 (2015) 276–285.
- [24] G. Bianchi, R. Cipollone, Theoretical modeling and experimental investigations for the improvement of the mechanical efficiency in sliding vane rotary compressors, *Appl. Energy*, 142 (2015) 95–107.
- [25] Y. Inaguma, A. Hibi, Vane pump theory for mechanical efficiency, *Proc. Inst. Mech. Eng., Part C, J. Mech. Eng. Sci.*, 219 (2005) 1269–1278.
- [26] J.P. MacHarg, Retro-fitting existing SWRO systems with a new energy recovery device, *Desalination*, 153 (2003) 253–264.
- [27] A.M. Gilau, M.J. Small, Designing cost-effective seawater reverse osmosis system under optimal energy options, *Renew. Energy*, 33 (2008) 617–630.
- [28] N. Kishizawa, K. Tsuzuki, M. Hayatsu, Low pressure multi-stage RO system developed in “Mega-ton Water System” for large-scaled SWRO plant, *Desalination*, 368 (2015) 81–88.